

## USE OF THE FRACTAL DIMENSION FOR POROSITY MODIFICATION IN ALUMINUM FOAMS MANUFACTURED USING SPACE HOLDER PARTICLES

Christian C. Reyes, Luis Béjar, Luis Pérez,  
Claudio Aguilar, Juan C. Carranza,  
Luis E. Carranza, and Ismeli Alfonso

**ABSTRACT.** The effect of space holder particles (SHP) fractal distribution on the porosity of aluminum foams manufactured by infiltration is studied in the present work. Physical models were used to estimate aluminum foam porosity, simulating SHP distribution for bimodal mixtures with different particle sizes and relative quantities. Results of these models were compared with mathematical models and the results obtained for experimental aluminum foams manufactured using a 332 Al-alloy base material and NaCl grains as SHP. Experimental foam structural characterization was carried out using image analysis to obtain porosity, density, wall thickness and fractal dimension, while mechanical characterization focused on the compressive Young modulus. Results show that it was possible to manufacture foams with different fractal porosities and a wide variety of unit cells, reaching a maximum of  $\sim 68\%$ . It was also found that pore wall thicknesses significantly decreased with the increase in the fine particles fraction. Besides, all the models presented a peak with a maximum porosity, whose values increased and shifted to low fine particles fraction with the increase in the sizes ratio. This behavior was also observed for the experimental foams with low particle size ratio. Nevertheless, for higher size ratios porosity showed an irregular behavior attributed to the mixing process.

### 1. Introduction

Metal foams acquired relevance for scientific research as functional and engineering materials just a few decades ago. First metal foams can be traced back to the 1920's decade when the first patent was registered in France in 1925, but it was not until the second half of the XX century that commercial manufacturing processes were developed, particularly during the 50's and 60's, followed by a second surge of new manufacturing processes during the 80's and 90's [1, 2]. Interest

---

2010 *Mathematics Subject Classification*: 74F10.

*Key words and phrases*: metal foams, aluminum alloys, fractals, Young modulus, advanced materials.

for metal foams is mainly attributed to their unique properties such as excellent strength-weight ratio, energy absorption, low density, high temperature operation and high stiffness. Additionally, metal foams can retain some characteristic properties from their base materials like good electrical and thermal conductivities, and weldability [3, 4]. Considering this, metal foams are suitable for a broad range of applications such as structural reinforcement and lightening, impact absorption, heat exchangers, dust and fluid filters, catalysts, components for structural damping, sound absorption, thermal insulation, and electromagnetic shielding [5]. These applications make possible their use for industries like automotive, aerospace, electronics, biomedicine, etc. Among the different metal foam fabrication methods currently available, infiltration through different space holder particles is well known for allowing great control over the number and size of pores within the metal matrix. This process proposed by Polonsky et al. in 1961 uses a removable volume of particles to create a preform of interconnected pores (depending on the process, particles may need to be sintered), followed by casting a metallic bath over the preform which gradually infiltrates the empty space. Once infiltration is completed, the molten metal solidifies and in the final stage the SHP are eliminated by different processes, usually dissolution or thermal degradation [6, 7]. The porosity of foams so obtained mainly depends on the SHP efficiency for filling a determined volume. Considering this, their size, quantity and distribution play a fundamental role in controlling foam structure and properties. Studies like [8, 9] demonstrate that using mixtures with different particle sizes helps to improve their packing density, finally contributing to obtaining a higher porosity. In fact, these works showed that maximum porosities for this process can only reach  $\sim 75\%$  when no sintering pressure is applied. This porosity is a direct result of the SHP packing, it being essential to control a mixture of different particle sizes and relative quantities for obtaining the desired porosity. The possible arrangements of the smaller particles in the spaces between the bigger ones is the cause of these differences in packing densities, which are affected mainly by two variables. The first one is the small particle relative quantity or proportion in the mixture. As this increases, small particles have better possibilities to fill voids, increasing packing density and reaching a maximum value. Nevertheless, as demonstrated by German et al. [10] and Ye et al. [11], there is a limiting condition given by a specific small particle proportion, and if it is exceeded, packing density diminishes gradually. The second variable is size ratio between the particles. As the size difference between big and small particles increases, the smaller ones can fill voids more easily. However, for this variable there is also a limiting condition. If an excessive size difference is observed, small particles are unable to hold their position in the voids and tend to accumulate in the bottom as demonstrated by Julien et al. [12].

Aluminum and its alloys, especially those with high silicon content, constitute an excellent material for infiltration foam manufacturing, since this alloying element provides high fluidity. Besides this, aluminum foams retain base alloy properties making them even more versatile materials, since they acquire properties like high ductility, non-toxicity, non-flammability, recyclability and corrosion resistance, making aluminum foams even lighter since aluminum alloys have low density [13].

As a result of their irregularity, structural characterization of porous materials represents a complex problem, since it is hard to describe using classical Euclidean geometry elements. Even if metal foams acquire a tridimensional body neither, none of their two phases (solid and porous) fully occupies the space, hence considering metal foams as a 3D object could be considered imprecise. Then, metal foams are better considered as objects with fractal dimensions lower than 3, the number which indicates the relation between the different characteristics of their pores, such as their relative sizes and quantities. Consequently, in recent years fractal geometry has become a useful tool for describing porous structure of metal foams. The concept of fractals enunciated by Cannon and Mandelbrot, is defined as an irregular geometrical shape that can be divided into smaller parts, with each of these being a copy of the original shape but in a lower scale [14]. Fractal dimension is a measure that indicates the grade complexity observed in a geometrical shape. In the case of porous materials this measure is affected by changes in structural characteristics like pore size and quantity, and interconnectivity [15], allowing us to determine the space occupied by the porous phase in a determined surface or volume with better precision. This is possible since fractional numbers can be used to represent a body's dimension unlike the topological geometry that only allows whole numbers. According to these remarks, this paper studies the SHP fractal distribution using different size and quantity conditions to determine their effect on the porosity of aluminum foams manufactured by infiltration. Physical and mathematical models were used for porosity estimation, comparing these estimations with the experimental values. Additionally, relations between fractal dimension, structure and properties were studied.

## 2. Experiment

**2.1. Physical Modeling.** Physical models were elaborated with the objective of predicting porosity simulating the conditions of the real infiltration method. Two known volumes (550 and 1300 cm<sup>3</sup>) were filled with bimodal mixtures of polymeric spheres (two different particle sizes) and three different fine-coarse particle combinations:  $\sim 0.5$ –1 mm, 0.5–1.5 mm, and 0.5–2 mm using layer accommodation to simulate SHPs mixture and distribution in the infiltration process. Subsequently, fine sand ( $\sim 100$   $\mu$ m in diameter particles) was poured over the spheres mixture, simulating the infiltration of molten aluminum. Two main parameters were measured for controlling the SHP distribution: i) sizes ratio  $R$ , representing the ratio between fine and coarse particles diameter ( $D_{\text{coarse}}/D_{\text{fine}}$ ), and ii) relative quantities  $C$  indicating the number of fine particles for each coarse particle in the mixture. It should be noted that results analysis was carried out calculating the volumetric fine particles fraction  $F$  corresponding to each value of relative quantities, since this facilitates data analysis and comparison with other works in literature. Every physical model consisted in the combination of one sizes ratio and one relative quantity. Three different sizes ratios were used ( $R = 2, 3, 4$ ) combined with relative quantities starting from 1:1 to maximum values of 1:40. This led to obtaining different fractal dimensions ( $D_f$ ), depicted in Table 1, and calculated from  $\log(\text{relative quantities})/\log(\text{sizes ratio})$ . This parameter is used for the study of the porous medium,

TABLE 1. List of physical models.

Model Code	Sizes ratio	Relative quantities (coarse:fine)	Fine particles fraction	Fractal dimension
M2-1	1	1:1	0.11	0.0
M2-2	2	1:2	0.20	1.0
M2-3	2	1:3	0.27	1.6
M2-4	2	1:4	0.33	2.0
M2-5	2	1:5	0.40	2.3
M3-1	3	1:2	0.07	0.6
M3-2	3	1:3	0.10	1.0
M3-3	3	1:4	0.13	1.3
M3-4	3	1:6	0.18	1.6
M3-5	3	1:7	0.21	1.8
M3-6	3	1:12	0.31	2.3
M3-7	3	1:18	0.40	2.6
M4-1	4	1:2	0.03	0.5
M4-2	4	1:4	0.06	1.0
M4-3	4	1:6	0.09	1.3
M4-4	4	1:8	0.11	1.5
M4-5	4	1:9	0.12	1.6
M4-6	4	1:10	0.14	1.7
M4-7	4	1:16	0.20	2.0
M4-8	4	1:27	0.30	2.4
M4-9	4	1:40	0.38	2.7

and as can be seen in Table 1 its value for relative quantities 1:1 is zero. Then, its study is really used for higher relative quantities, indicating the complexity of the porous system.

Particle packing densities were measured for every model by calculating the volumetric fraction using Equation 1, where  $\gamma$  is packing density (expressed in %),  $V_M$  the volume of the spheres mixture and  $V_S$  is the volume of the infiltrated sand.

$$(2.1) \quad \gamma = \frac{V_M}{V_M + V_S} \times 100$$

A mathematical model developed by Yang [16] was used as a reference and for comparison purposes based on Larrard [17], and Chang and Meidani Method for packing density estimation [18]. This model uses a set of equations (2.2)–(2.7) to predict the minimum void ratio in a bimodal particle mixture. These equations consider two physical effects that affect packing density to improve accuracy of calculations. The first one, known as “wall effect”, takes place when a big particle is surrounded by many small particles whose own interaction prevents them from contacting the big particle, increasing empty space. The second one is “loosening effect” and occurs when a small particle tries to fill a void between big particles, but

this one is not big enough for the particle to fit, hence the small particle displaces the big ones, increasing empty space in the mixture.

The mathematical model uses Equations (2.2) and (2.3) to calculate the mixture minimum void ratios ( $\hat{e}_1$  and  $\hat{e}_2$ ), considering respectively the loosening effect [ $l(r)$ ], and the wall effect [ $w(r)$ ], which can be calculated using Equations (2.4) and (2.5), respectively. These equations take into account two components (particles) of different sizes,  $r$  being the size ratio between fine and coarse particles. Otherwise,  $e_1$  and  $e_2$  are, respectively, the minimum void ratios for coarse and fine particles (without interaction between them). The true void ratio is affected by the loosening effect due to small size particles, and the wall effect due to larger size particles [18]. That is why  $y_2$  (fine particles fraction) and  $y_1$  (coarse particles fraction) are included in each equation in that order. In Equation (2.6)  $e$  represents the maximum value between  $\hat{e}_1$  and  $\hat{e}_2$ , which is used to calculate mixture fractional packing density ( $\gamma$ ) through Eq. (2.7) ( $\times 100$  for percentage).

$$(2.2) \quad \hat{e}_1 = e_1 - [1 + e_1 - l(r)(1 + e_2)y_2]$$

$$(2.3) \quad \hat{e}_2 = e_2 - [e_2y_1 - w(r)e_2y_1]$$

$$(2.4) \quad l(r) = \sqrt{1 - (1 - r)^{1.02}}$$

$$(2.5) \quad w(r) = 1 - (1 - r)^{1.5}$$

$$(2.6) \quad e = \text{Max}(\hat{e}_1, \hat{e}_2)$$

$$(2.7) \quad \gamma = \frac{1}{e + 1}$$

**2.2. Aluminum foam fabrication.** Aluminum foams were manufactured using 332-aluminum alloy as the base material, with a chemical composition depicted in Table 2. As can be seen, Si content is high, which favors the fluidity of the molten alloy through the empty spaces of the SHP.

TABLE 2. Real aluminum alloy 332 chemical composition.

Element	Si	Cu	Fe	Mn	Zn	Ti	Mg	Al
% Weight	10.21	3.25	1.15	0.95	0.81	0.13	0.01	Balance
% Atomic	10.21	1.43	0.58	0.48	0.35	0.08	0.01	Balance

Common commercial salt (NaCl) grains were used as SHP as they have a higher melting temperature than aluminum and are also easily removable by dissolution in water. NaCl particles were sieved and separated into three average sizes: 1 mm, 2 mm, and 4 mm. These particles were mixed using relative quantities of  $C = 1, 2, 4,$  and  $6$  for the size ratio  $R = 2$ ; and  $C = 2, 4, 6, 8, 10,$  and  $12$  for the size ratio  $R = 4$ . Figure 1a shows examples of these NaCl particles of different sizes, while Figure 1b to d shows representations of different expected unit cells, which characterizes the distribution after mixing. Each particle or unit cell is in contact with its neighbors,

a fact that leads to their superposition and modifies packing. Although NaCl are irregular, their analysis revealed that their shape factor ( $F$ ) is near 1.0. Also known as circularity,  $F$  is a dimensionless parameter used for analyzing irregular particles, defined not only by the area of a particle but also by its  $p$  perimeter. A perfect circle will have a shape factor of 1.0, while a value near 0 indicates a more irregular or elongated shape [19]. The irregular shape of NaCl is expected to influence packing, a fact that will be discussed once the results have been obtained and compared to the packing of the spherical particles used in the physical models.

Figures 2a and 2b shows the irregular arrangements of the smaller particles in the spaces between the bigger ones for the physical models (Figure 2a) and NaCl (Figure 2b), where packing is different according to the roundness for complete spherical (physical models) and irregular particles (NaCl).

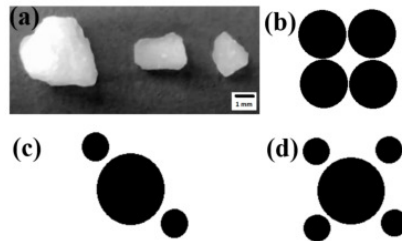


FIGURE 1. (a) Optical image of NaCl particles, with average sizes close to 4 mm, 2 mm, and 1 mm. (b-c) Expected unit cells for the cases of: (b) only particles of 4 mm (non-fractal), (c) 2 particles of 2 mm per one particle of 4 mm ( $D_f = 1$ ), and (d) 4 particles of 2 mm per one particle of 4 mm ( $D_f = 2$ ).

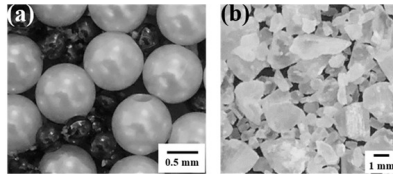


FIGURE 2. Possible arrangements for space holder particles. (a) Spherical particles. (b) Irregular particles.

Rounded spheres of the physical models are expected to present higher packing values compared to those obtained by SHPs. Cho et al. [19] identified three structural characteristics that affect packing density: sphericity, roundness, and smoothness. Sphericity refers to the grade of similarity between a particle and a sphere considering their length, height, and width; those particles with a shape closer to a sphere generate ordered arrangements with better distribution, reducing packing defects (wall and loosening effects) and, as a consequence, increasing packing density. This is shown in works like the ones by Pu et al. [20] and Fei et al. [21].

Roundness is defined as the ratio of the average radius of curvature in corners to the radius of inscribing circle. Higher roundness particles have better mobility, which allows them to adopt closer positions to each other, raising packing density. In contrast, highly angular particles tend to favor packing defects but have better connectivity since they have more contact points between them. Particle smoothness describes its surface texture, and this structural characteristic behaves in a similar way to roundness, since smooth surface particles have better mobility because there is low friction between them, achieving better packing densities in comparison with rough surface particles [19, 21].

Fabrication process was completed using an infiltration device developed and patented by our research team [Mexican Patent, MX/a/2017/010803, 09/23/2017]. It consists of a 5 cm diameter and 30 cm height AISI 314 stainless steel cylinder with a sealed base. For infiltration NaCl particles were introduced in the cylinder (NaCl filled 10 cm as a preform), and at the top of this preform the Al-Si-Cu alloy was introduced. The cylinder was then sealed at the top and introduced into a Prefinsa HR-C4 electric resistance furnace at 700 °C. At this temperature NaCl preforms were infiltrated by gravity by the quaternary alloys. The cylinder was extracted from the furnace and air cooled. Resulting Al alloys-NaCl composites were removed from the steel cylinder and immersed in water for 5 hours to dissolve NaCl, the experimental Al foams being obtained. Under certain circumstances and depending on the combination of NaCl particles, Argon injection was necessary to ensure a complete infiltration, using an initial 10 ft<sup>3</sup>/h flow and increasing an amount of 10 ft<sup>3</sup>/h in 30-second intervals until a maximum flow of 50 ft<sup>3</sup>/h.

**2.3. Aluminum foam characterization.** Structural characterization of the experimental foams was carried out using samples with an approximated diameter of 50 mm and height of 30 mm. These samples were analyzed by visual and stereoscopic inspection using a Motic-SMZ-168-BP stereoscope. Structural analysis focused on measuring aluminum foam density, porosity, wall thickness and fractal dimension. Foam samples mass and volume were measured to calculate density. Porosity was calculated based on their density using Equation 8 proposed by Wang et al. [6], where  $\rho_{Al}$  and  $\rho_f$  are aluminum and foam densities, respectively.

$$(2.8) \quad \% \text{ Porosity} = \frac{\rho_{Al} - \rho_f}{\rho_{Al}} \times 100$$

Wall thickness was obtained through image analysis from different foams' cross sections. Using ImageJ software [22], lines were drawn on foams' cross-sectional faces, measuring and averaging all the wall segments touched by them. Fractal dimension was also measured using foams' cross sectional images that were analyzed with an ImageJ fractal dimension tool, which automatically calculates it by box counting method. These results were compared to the expected values obtained through  $\log(\text{relative quantities})/\log(\text{sizes ratio})$  obtained from the SHP mixtures. The analysis of  $D_f$  using images not only reveals the effect of the fractal mixture but also the complexity of the structure, including aspects such as the morphology of the pores, the total area that they occupy and the distance between them.

On the other hand, mechanical characterization required machining operations in order to obtain samples with a diameter of 30 mm and a height of 25 mm, according to ASTM E9-09 “Standard Test Methods of Compression Testing of Metallic Material at Room Temperature”. Compression Tests were performed at a constant strain speed of 5 mm/s.

### 3. Results and discussion

**3.1. Physical modeling.** Figure 3 shows packing density results obtained from the physical models, for the three analyzed sizes ratios. It can be observed that packing density presents a rising tendency as the fine particles fraction increases, reaching a maximum value, and then decreasing even with the increase in the fine particles fraction.

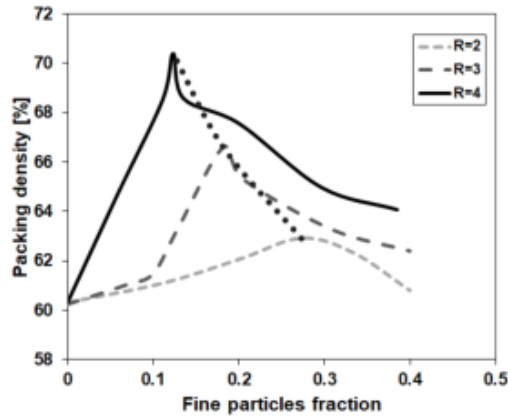


FIGURE 3. Packing density-particles fraction relation for the physical model

This behavior completely agrees with the results reported by Groot and Stoyanov, [23] and can be explained because fine particles fill the empty voids left by the bigger particles. As the fine particles fraction increases, empty space reduces to a minimum, reaching the maximum packing density in a determined fine-coarse particles proportion. After this point increasing fine particles quantity leads to a decreasing tendency in packing density, since voids between fine particles cannot be filled by coarse particles, and, consequently, empty space increases, reducing packing density. Related to the higher packing density with the increase in the size ratio, a plausible explanation is that a bigger size difference between fine and coarse particles helps the smaller ones to introduce themselves into the voids formed by coarse particles. Additionally, it can be noted that maximum packing density is found in lower fine particles fractions as the mixture size ratio increases. This happens because smaller fine particles are more efficient in filling empty space, so a lower volumetric fraction is needed to reach maximum packing density.

**3.2. Aluminum Foams.** Figure 4a to 4f shows examples of obtained aluminum foams corresponding to sizes ratios  $R = 2$  (subsections a to c) and  $R = 4$  (subsections d to f) modifying the relative quantities. All the foams showed open porosity with interconnected and homogeneously distributed pores.

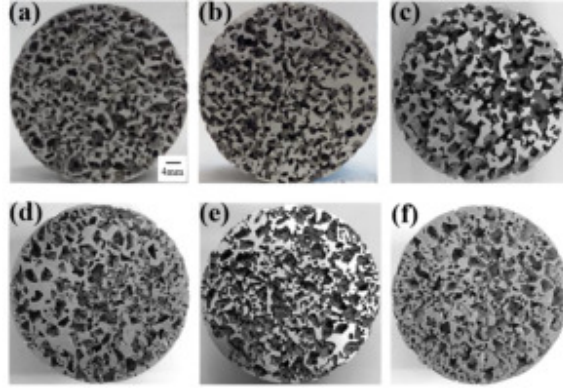


FIGURE 4. Examples of aluminum foam samples. (a) Foam E-2 with  $R = 2$   $C = 2$   $F = 0.2$  [24]. (b) Foam E-3 with  $R = 2$   $C = 4$   $F = 0.33$  [24]. (c) Foam E-4 with  $R = 2$   $C = 6$   $F = 0.42$ . (d) Foam E-6 with  $R = 4$   $C = 2$   $F = 0.05$ . (e) Foam E-8 with  $R = 4$   $C = 8$   $F = 0.11$ . (f) Foam E-10 with  $R = 4$   $C = 12$   $F = 0.15$

Figure 5a to 5d shows the analysis of the individual cells for the experimental foams. This study was carried out for a better observation of the porosity distribution. Although the distribution of unit cells was not exactly done in this way, these images help to observe how it was the arrangement of the SHPs of different sizes for different relative quantities of small-big particles. For example, Figure 5a shows a big pore surrounded by 2 smaller ones, while Figure 5d shows a big pore surrounded by 8. This behavior confirms the predictions presented in Table 1 and Figure 1b to 1c.

Figure 6a and 6b shows the results of porosity and wall thickness for the experimental foams manufactured using different values of relative quantities ( $C$ ) and sizes ( $R$ ). There were included both fine particles fraction on the  $X$ -axis and fractal dimension in parentheses, measured according to  $C$  and  $R$ . As can be observed in Figure 6a, porosity for  $R = 2$  presents a maximum for a value of fine particles fraction ( $F$ ) of 0.2, decreasing for higher values of  $F$ . This behavior is similar to that obtained for the physical models already observed in Figure 3. Otherwise, for  $R = 4$  the behavior was irregular, increasing and decreasing in a successive manner as the SHP fine particles fraction increases. This irregular behavior is related to the mixture: the rising tendency occurs because fine particles occupy the voids formed between coarse particles. However, since SHP mixing is not perfect, fine particles cannot always fill the hollow space. On the contrary, sometimes they can take undesirable positions separating the coarse particles or forming particle accumulations

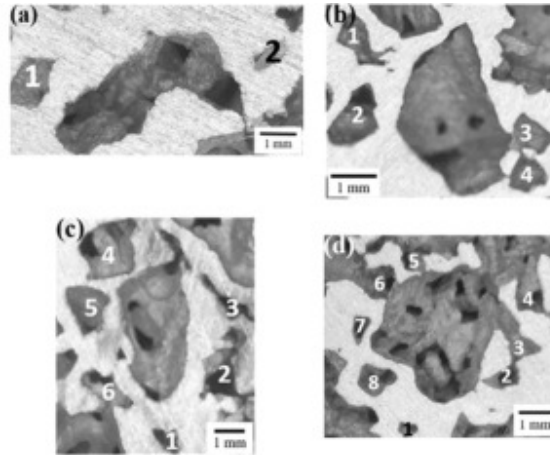


FIGURE 5. Unit cells obtained from metal foams (coarse particles:fine particles). (a) 1:2. (b) 1:4. (c) 1:6. (d) 1:8.

reducing packing density, as reported by Kong and Lanutti [25]. Hence, even if an initial increment of fine particles for each coarse particle can raise foam porosity percentage, adding more fine particles does not imply that porosity maintains a rising tendency. On the contrary, increasing fine particle number in the mixture gives them more possibilities of filling empty space between coarse particles, making it possible to reach maximum packing density. Figure 6b depicts the behavior for wall thickness, showing a decreasing tendency as the fine particles fraction and sizes ratio increase. This is also explained because fine particles fill empty space between coarse particles, reducing empty space between SHP and consequently generating thinner walls. Nevertheless, in this case descending tendency persists even if the fine particles fraction exceeds the proportion for which maximum packing density is found. This can be explained since the voids between fine particles are smaller in comparison with those from coarse particles or fine-coarse mixtures.

Figure 6c and 6d presents the relations between the fractal dimension (determined using images) and porosity (Figure 6c) and cell wall thickness (Figure 6d). In this case no independent values of  $R$  were used (as in Figures 6a and b), only considering the dependence on fractal dimension ( $D_f$ ) obtained by image analysis for both graphs. As can be seen a rising tendency is observed for porosity (Figure 6c); an expected fact due to fractal dimension is a measure of the amount of space occupied by pores in the aluminum foam. On the contrary, Figure 6d shows that it was not possible to find a tendency for cell wall thickness. Considering that the fractal dimension was measured in a 2D space represented by the aluminum foams faces, if its value is closer to 2, that is an indicator that pores tend to occupy the whole surface. On the other hand, if the fractal dimension is closer to 1, fewer pores will be found and the metallic phase will be predominant on the surface. These Figures show that the use of one or other value of  $D_f$  can be useful according to the different relations that are established.

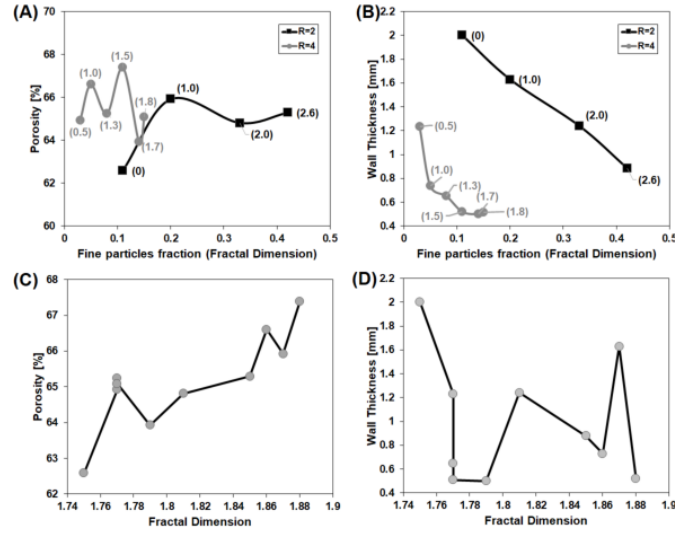


FIGURE 6. (a) Porosities of the aluminum foams for different mixtures of space holder particles, and (b) Wall thickness results. Porosity (c) and wall thickness (d) dependences with fractal dimension

**3.3. Comparison between experimental foams and models.** For comparative purposes, the effect of size ratio and relative quantities on packing (or porosity) were analyzed for the experimental foams compared to the physical and mathematical models presented in this work. This study is presented in Figure 7a and 7b, where it is observed that porosity values are higher for the cases where a higher size ratio was used ( $R = 4$ ). Besides, maximum porosities were found for lower fine particles fractions compared to the case of  $R = 2$ . It was observed that the physical model constitutes a better approximation to the real foam than the mathematical model. For the case of  $R = 2$ , foam presents an error of 3% in maximum porosity estimation compared to the physical model, while compared to the mathematical one the error was near 4%. For  $R = 4$ , the physical model shows once again an error of 3%, but the error for the mathematical model reached 6.4%. This behavior was repeated for the maximum porosity fine particles fraction ( $F = 0.1-0.3$ ), but errors were higher. For  $R = 2$ , the physical model presents an error of 7% and the mathematical one an error of 12%. For  $R = 4$ , the error significantly reduced for the physical model reaching a value of 1%. In contrast, for the mathematical model the error increased to 18%.

These errors were expected due to different causes. First, porosities predicted by mathematical models are maximum since they establish a perfect mixture and accommodation of the particles considering ideal packing conditions in which empty space between particles is minimum. On the other hand, although physical model behavior is similar to that of the mathematical model, their porosities are lower

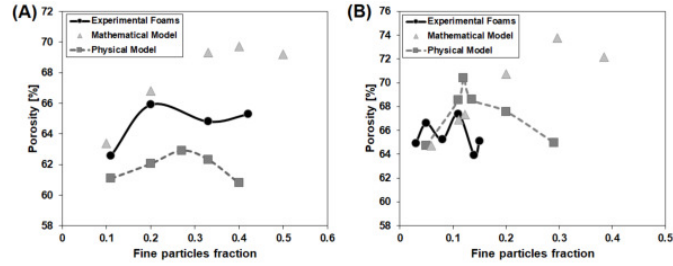


FIGURE 7. Comparison of experimental foams with physical and mathematical models for: (a) Size ratio  $R = 2$ . (b) Size ratio  $R = 4$

due to imperfect mixtures. Besides, maxima of the mathematical model are presented at higher values of  $F$  compared to physical models due to the minimum void ratio condition. Since the mathematical model considers ideal particle packing, the arrangement of the coarse particles is ordered generating voids with uniform size and distribution that require a higher number of fine particles to achieve maximum packing density. In contrast, packing imperfections in physical models and experimental foams generate irregular distribution of coarse particles, which means that less fine particles fraction is needed in the mixture to achieve maximum packing. Differences are also present because particles volume calculation is not exact, since it is difficult to control the number of spheres required to completely fill control volume without exceeding or not filling recipient's maximum capacity. Finally, the shape of the SHP used for foams manufacturing is irregular, they can present incipient melting (sintering) and leave a lower volume compared to that obtained in the physical model.

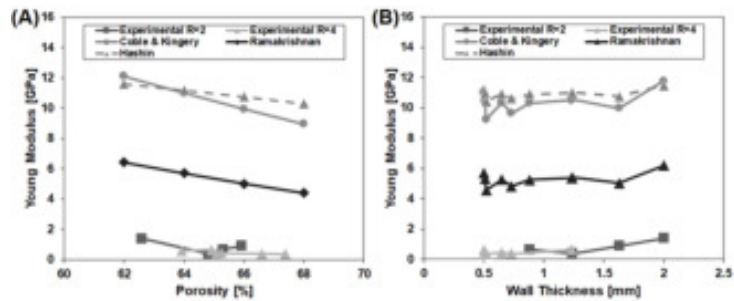


FIGURE 8. (a) Effect of porosity on the Young modulus for experimental foams and mathematical models in literature. (b) Effect of the foam wall thickness on the Young Modulus

**3.4. Aluminum foams mechanical characterization.** Figure 8a shows a comparison between the experimental Young modulus and different three mathematical models as a reference, Coble and Kingery, [26] Ramakrishnan, [27] and

Hashin [28]. The Young modulus showed a decreasing tendency for both experimental foams and mathematical models as porosity increases, which agrees with the expected results for the effective elastic modulus according to Nemat-Nasser and Hori [29]. Consequently, the lowest Young modulus coincides with the maximum porosity,  $E$  being slightly higher for the foams with  $R = 2$ . This tendency is slightly detected for the foams because their mechanical properties are affected not only by the porosity but also by cell wall thickness, while mathematical models consider porosity as the only property affecting the Young modulus. This dependence on cell wall thickness is observed in Figure 8b, where the observed tendency is the increase in the Young modulus with the increase in cell wall thicknesses, although the results for mathematical models show irregular behaviors. As cell walls are thinner, they become less resistant to compressive strength.

#### 4. Conclusions

Space holder particles distribution is a key factor for aluminum foams fabricated by infiltration methods since porosity highly depends on it and by extension their mechanical properties.

The use of different space holder particles sizes improves porosity distribution; as size difference between fine and coarse particles is bigger, porosity slightly increases.

Relatives quantities between fine and coarse particles and their corresponding fine particles fraction are fundamental to obtaining the best possible porosity distribution for different space holder mixtures.

Size ratio and fine particles fraction have a huge influence over wall thickness for experimental foams.

The physical model constitutes a good first approach for porosity prediction, and even if it is not fully accurate, it is a good approximation for foams maximum porosity and its corresponding fine particles fraction.

Fractal dimension demonstrated to be a useful parameter to describe a porous structure since it is strongly related to porosity, making it possible to describe porous phase distribution using a single numerical value instead of describing it using size and particle quantity.

**Acknowledgments.** Christian Reyes wants to acknowledge the financial support through the scholarship for doctoral studies (893763) from Consejo Nacional de Ciencia y Tecnología (CONACYT) and academic support from Universidad Michoacana de San Nicolás de Hidalgo (UMSNH), Universidad Autónoma de México (UNAM) and Universidad Técnica Federico Santa María (UTSM). Ismeli Alfonso would like to acknowledge the financial support from CONACYT (SEP CONACYT 285215) and Universidad Nacional Autónoma de México (UNAM PAPIIT IN117316).

## References

1. S. Singh, N. Bhatnagar, *A survey of fabrication and application of metallic foams (1925–2017)*, Journal of Porous Materials **25** (2018), 537–554.
2. J. Banhart, G. S. Vinod-Kumar, P. H. Kamm, T. R. Neu, F. García-Moreno, *Special issue on cellular materials light-metal foams: Some recent developments*, Ciencia & Tecnología dos Materiais **28** (2016), 1–4.
3. D. Potočník, B. Razboršek, F. Mirko, *Overview of aluminum foam machining*, Proceedings of the 12<sup>th</sup> International Symposium on Exploitation of Renewable Energy Sources and Efficiency, 2016, 361–376.
4. J. Marx, A. Rabiei, *Overview of composite metal foams and their properties and performance*, Advanced Engineering Materials **19** (2017), 1600776.
5. F. García-Moreno, *Commercial applications of metal foams: Their properties and production*, Materials **9** (2016), 85.
6. Z. Wang, J. Gao, K. Chang, L. Meng, N. Zhang, Z. Guo, *Manufacturing of open-cell aluminum foams: Via infiltration casting in super-gravity fields and mechanical properties*, RSC Advances **8** (2018), 15933–15939.
7. J. Banhart, *Manufacture, characterization and application of cellular metals and metal foams*, Progress in Materials Science **46** (2001), 559–632.
8. R. K. Mcgeary, *Mechanical packing*, Journal of the American Ceramic Society **44** (1961), 513–522.
9. C. S. Chang, J. Y. Wang, L. Ge, *Modeling of minimum void ratio for sand-silt mixtures*, Engineering Geology **196** (2015), 293–304.
10. R. German, S. J. Park, *Handbook of Mathematical Relations in Particulate Materials Processing*, Wiley-Interscience, USA, 2008, 20–21.
11. X. Ye, Y. Li, Y. Ai, Y. Nie, *Novel powder packing theory with bimodal particle size distribution-application in superalloy*, Advanced Powder Technology **29** (2018), 2280–2287.
12. P. Y. Julien, Y. Lan, G. Berthault, *Experiments on stratification of heterogeneous sand mixtures*, Bulletin de la Société Géologique de France **164** (1993), 649–660.
13. D. K. Rajak, L. A. Kumaraswamidhas, S. Das, *Technical overview of aluminum alloy foam*, Reviews on Advanced Materials Science **48** (2017), 68–86.
14. J. W. Cannon, B. B. Mandelbrot, *The fractal geometry of nature*, Am. Math. Mon. **91** (1984), 594.
15. L. Pérez, S. Lascano, C. Aguilar, D. Domancic, I. Alfonso, *Simplified fractal FEA model for the estimation of the Young's modulus of Ti foams obtained by powder metallurgy*, Materials & Design **83** (2015), 276–283.
16. Z. Yang, *Study of Minimum Void Ratio for Soils with a Range of Grain-Size Distributions*, PhD Thesis, 2013.
17. F. Larrard, *Concrete Mixture Proportioning: A Scientific Approach*, (2011 Ed.), E & FN SPON, New York.
18. C. Chang, M. Meidani, *Dominant grains network and behavior of sand-silt mixtures: Stress-strain modeling*, Int. J. Numer. Anal. Methods Geomech. **37** (2013), 2563–2589.
19. G.-C. Cho, J. Dodds, J. C. Santamarina, *Particle shape effects on packing density, stiffness, and strength: Natural and crushed sands*, Journal of Geotechnical & Geoenvironmental Engineering **132** (2016), 591–602.
20. W. Pu, J. Li, X. He, J. Ying, C. Jiang, C. Wan, *Controlled crystallization of spherical active cathode materials for NiMH and Li-ion rechargeable batteries*, Journal of New Materials for Electrochemical Systems **8** (2005), 235–241.
21. W. Fei, G. A. Narsilio, *Impact of three-dimensional sphericity and roundness on coordination number*, Journal of Geotechnical & Geoenvironmental Engineering **146** (2020), 06020025.
22. W. S. Rasband, *ImageJ*, <http://imagej.nih.gov/ij/>, 2005, Accessed: 01.10.2020.
23. R. D. Groot, S. D. Stoyanov, *Close packing density and fracture strength of adsorbed polydisperse particle layers*, Soft Matter **7** (2011), 4750–4761.

24. J. C. Carranza, L. Pérez, R. Ganesan, B. Y. Casas, R. A. L. Drew, C. Aguilar, I. A. Figueroa, I. Alfonso, *Effect of fractal distribution of the porosity on mechanical properties of Al foams manufactured by infiltration*, Journal of the Brazilian Society of Mechanical Sciences and Engineering **41** (2019).
25. C. M. Kong, J. J. Lannutti, *Effect of agglomerate size distribution on loose packing fraction*, Journal of the American Ceramic Society **83** (2004), 2183–2188.
26. R. L. Cobel, W. D. Kingery, *Effect of porosity on physical properties of sintered alumina*, Journal of the American Ceramic Society **39** (1965), 377–385.
27. N. Ramakrishnan, V. S. Arunachalam, *Effective elastic moduli of porous solids*, Journal of Materials Science **25** (1990), 3930–3937.
28. Z. Hashin, *The elastic moduli of heterogeneous materials*, J. Appl. Mech. **29** (1962), 143–150.
29. S. Nemat-Nasser, M. Hori, *Micromechanics: Overall Properties of Heterogeneous Materials*, (2<sup>nd</sup> rev. ed.), Elsevier, Amsterdam.

## КОРИШЋЕЊЕ ФРАКТАЛНЕ ДИМЕНЗИЈЕ ЗА ПРОМЕНУ ПОРОЗНОСТИ У АЛУМИНИЈУМСКИМ ПЕНАМА

РЕЗИМЕ. У овом раду проучаван је ефекат фракталне расподеле честица носиоца простора (SHP) на порозност алуминијумских пена произведених инфилтрацијом. Коришћени су физички модели за процену порозности алуминијумске пене, симулирајући расподелу SHP за бимодалне смеше са различитим величинама честица и релативним количинама. Резултати ових модела упоређивани су са математичким моделима и резултатима добијеним за експерименталне алуминијумске пене произведене од основног материјала легуре 332 Al и зрна NaCl као SHP. Експериментална структурна карактеризација пене изведена је анализом слике како би се добила порозност, густина, дебљина зида и фрактална димензија, док је механичка карактеризација усусређена на Јунгов модул при сажимању. Резултати показују да је било могуће произвести пене са различитим фракталним порозностима и широким спектром јединичних ћелија, достигавши максимум од  $\sim 68\%$ . Такође је утврђено да се дебљина зида поре значајно смањује са повећањем односа финих честица. Поред тога, сви модели су показали пик са максималном порозношћу, чије су се вредности повећавале и померале у област ниских односа финих честица са повећањем односа величина. Ово понашање је примећено и код експерименталних пена са малим односом величине честица. Ипак, за веће односе величине порозност је показала неправилно понашање које је приписано процесу мешања.

Department of Mechanical Engineering  
Universidad Michoacana de San Nicolás de Hidalgo  
Morelia  
Mexico  
[christian\\_reyes\\_olivo@hotmail.com](mailto:christian_reyes_olivo@hotmail.com)

(Received 29.01.2021.)  
(Revised 17.04.2021.)  
(Available online 11.06.2021.)

Department of Mechanical Engineering  
Universidad Michoacana de San Nicolás de Hidalgo  
Morelia  
Mexico  
[luis.bejar@umich.mx](mailto:luis.bejar@umich.mx)

Department of Mechanical Engineering  
Universidad Técnica Federico Santa María  
Valparaiso  
Chile  
[luis.perez@usm.cl](mailto:luis.perez@usm.cl)

Department of Metallurgy and Materials  
Universidad Técnica Federico Santa María  
Valparaiso  
Chile  
[claudio.aguilar@usm.cl](mailto:claudio.aguilar@usm.cl)

Instituto de Investigaciones en Materiales Unidad Morelia  
Universidad Nacional Autónoma de México  
Morelia  
Mexico  
[JcarranzaG@outlook.com](mailto:JcarranzaG@outlook.com)

Department of Mechanical Engineering  
Universidad Michoacana de San Nicolás de Hidalgo  
Morelia  
Mexico  
[enreek\\_95@hotmail.com](mailto:enreek_95@hotmail.com)

Instituto de Investigaciones en Materiales Unidad Morelia  
Universidad Nacional Autónoma de México  
Morelia  
Mexico  
[ialfonso@iim.unam.mx](mailto:ialfonso@iim.unam.mx)